



UNIVERSITY OF LEEDS

This is a repository copy of *Short-wave infrared LEDs from GeSn/SiGeSn multiple quantum wells*.

White Rose Research Online URL for this paper:

<http://eprints.whiterose.ac.uk/109875/>

Version: Accepted Version

Article:

Stange, D, von den Driesch, N, Rainko, D et al. (8 more authors) (2017) Short-wave infrared LEDs from GeSn/SiGeSn multiple quantum wells. *Optica*, 4 (2). pp. 185-188.

<https://doi.org/10.1364/OPTICA.4.000185>

© 2017 Optical Society of America. One print or electronic copy may be made for personal use only. Systematic reproduction and distribution, duplication of any material in this paper for a fee or for commercial purposes, or modifications of the content of this paper are prohibited.

Reuse

Items deposited in White Rose Research Online are protected by copyright, with all rights reserved unless indicated otherwise. They may be downloaded and/or printed for private study, or other acts as permitted by national copyright laws. The publisher or other rights holders may allow further reproduction and re-use of the full text version. This is indicated by the licence information on the White Rose Research Online record for the item.

Takedown

If you consider content in White Rose Research Online to be in breach of UK law, please notify us by emailing eprints@whiterose.ac.uk including the URL of the record and the reason for the withdrawal request.

SHORT-WAVE INFRARED LEDs FROM GeSn/SiGeSn MULTIPLE QUANTUM WELLS

DANIELA STANGE,^{1,*} NILS VON DEN DRIESCH,¹ DENIS RAINKO,¹ SØREN ROESGAARD,^{1,2} IVAN POVSTUGAR,³ JEAN-MICHEL HARTMANN,⁴ T. STOICA,⁵ ZORAN IKONIC,⁶ SIEGFRIED MANTL,¹ DETLEV GRÜTZMACHER,¹ AND DAN BUCA¹

¹Peter Grünberg Institut 9 and JARA-Fundamentals of Future Information Technologies, Forschungszentrum Jülich, 52425 Jülich, Germany

²Interdisciplinary Nanoscience Center (iNANO), Aarhus University, DK-8000 Aarhus, Denmark

³Central Institute for Engineering, Electronics and Analytics (ZEA), Forschungszentrum Jülich, 52425 Jülich, Germany

⁴Univ. Grenoble Alpes F-38000 and CEA, LETI, MINATEC Campus, F-38054 Grenoble, France

⁵National Institute of Materials Physics, P.O. Box MG-7, Magurele, Bucharest 077125, Romania

⁶Institute of Microwaves and Photonics, School of Electronic and Electrical Engineering, University of Leeds, Leeds LS2 9JT, United Kingdom

*Corresponding author: d.stange@fz-juelich.de

Group IV photonics is on the way to be integrated with electronic circuits, making information transfer and processing faster and more energy efficient. Light sources, a critical component of photonic integrated circuits, are still in development. Here, we compare Multi-Quantum-Well (MQW) light emitting diodes (LEDs) with $\text{Ge}_{0.915}\text{Sn}_{0.085}$ wells and $\text{Si}_{0.1}\text{Ge}_{0.8}\text{Sn}_{0.1}$ to a reference $\text{Ge}_{0.915}\text{Sn}_{0.085}$ homojunction LED. Material properties as well as band structure calculations are discussed, followed by optical investigations. Electroluminescence spectra acquired at various temperatures indicate an effective carrier confinement for electrons and holes in the GeSn quantum wells and confirm the excellent performance of GeSn/SiGeSn MQW light emitters.

The integration of optical circuits into everyday electronic systems is driven by the need for an effective reduction of energy consumption. Replacing copper wires partly by optical interconnects would strongly reduce heat dissipation - crucial for high performance nanoscale devices, and simultaneously solve the electronic modulation bandwidth bottleneck¹. The industry standard wavelength range for telecommunication lies in between 1.3 μm and 1.6 μm, where optical components based on Si and Ge are already available but could be expanded to higher wavelength in future². Yet, the fabrication of an on-chip light source poses challenges. Advanced materials like III-V semiconductors offer suitable properties for light emission, but integration into Si technology is cost-intensive and yet suffers on too low yield in terms of wafer bonding on silicon. Group IV semiconductors, on the other hand, lack emission efficiency due to their indirect bandgap. This major drawback has been overcome by alloying Ge with Sn, which offers the possibility to tune the bandgap of Ge, shifting it to lower energies³. The lowering occurs faster for Γ- than for L-valley, and therefore, the indirect semiconductor Ge turns into a fundamental direct bandgap semiconductor GeSn⁴. Thus, lasing action has already been demonstrated for GeSn layers with Sn contents above 8.5% in Fabry-Perot and micro cavity resonators^{4,5}. Another set of group IV alloys, ternary SiGeSn, extend Sn-based material properties, offering additional degrees of freedom in the design of group IV heterostructures. The combination of GeSn and SiGeSn can expand the range of accessible wavelengths, and therefore, the range of applications of integrated optical chips on the powerful silicon microelectronic platform. Recent developments in the growth of group IV hetero- and quantum-structures also offer the possibility of using these low-dimensional structures for other (opto-) electronic applications⁶, and even in quantum computing.

In this article we demonstrate the advantages of (Si)GeSn heterostructures for light emitting devices. GeSn alloys as active material for light emitting diodes (LEDs) have already been investigated, but up to now the breakthrough to efficient LEDs or electrically pumped lasing is still missing. Approaches using GeSn homojunctions with Sn concentrations up to 12%⁷ lead to an increased emission compared to elemental Ge diodes⁸. The implementation of hetero- and multi-quantum-well (MQW) structures with GeSn wells and Ge barriers did not enhance significantly light emission or decreased current density compared to simple homojunction devices⁹⁻¹¹. Due to established light emitters from III-V materials, it is well-known that quantum structures can lead to lower lasing threshold current densities by several orders of magnitude¹². The carrier confinement inside direct bandgap GeSn wells is weak when Ge is used as a barrier material, leading either to a lack of type-I band alignment or to small barrier heights, of the order of $k_B T$, ~25 meV at room temperature¹¹. Switching from Ge to SiGeSn ternary alloys would, provided that the Si and Sn atomic concentrations are properly chosen¹³, offer much stronger carrier confinement and type I band alignment. However, uncertainties concerning the SiSn bowing parameter make the calculations of GeSn/SiGeSn band alignment unreliable. Depending on the $b_{\text{SiSn},\Gamma}$ value, which varies in literature between 3.9¹⁴ and 24¹⁵⁻¹⁷, the very same GeSn/SiGeSn heterostructure can offer either a strong type II band alignment (confinement of electrons and holes in different layers) or a strong type I alignment (carrier confinement in the GeSn well). The only way to verify that carriers are efficiently trapped in GeSn quantum wells, is the experimental fabrication of such GeSn/SiGeSn LEDs and study of their electroluminescence properties. Hence, we investigate experimentally the influence of SiGeSn barriers in a GeSn/SiGeSn MQW LED, and compare it to homojunction GeSn LEDs, based on electroluminescence performance. Following this idea, we have fabricated LEDs from a $\text{Ge}_{0.914}\text{Sn}_{0.086}/\text{Si}_{0.105}\text{Ge}_{0.786}\text{Sn}_{0.109}$ MQW stack. The heterostructure was grown by reactive gas source epitaxy⁴. The LED structure

was deposited on a 2.7 μm thick Ge buffer on top of a 200 mm Si(001) wafer¹⁸ in a single epitaxial run. A 280 nm thick partially relaxed n-type doped $\text{Ge}_{0.914}\text{Sn}_{0.086}$ buffer was first grown (Phosphorus, $\sim 3 \cdot 10^{19} \text{ cm}^{-3}$). It sets the residual compressive strain in the GeSn wells coherently grown on top to -0.24% only (which is beneficial in terms of bandgap directness). The PH₃ precursor flux was stopped 60 nm before the first SiGeSn barrier to avoid any unintentional doping of the active layers. The quantum wells (GeSn) and barriers (SiGeSn) are lattice matched, whereas the absolute strain in the SiGeSn barriers amounts to -0.09%, meaning that the material is almost strain-free. The LED structure is completed by a p-doped $\text{Ge}_{0.915}\text{Sn}_{0.085}$ layer (Boron, $\sim 7 \cdot 10^{18} \text{ cm}^{-3}$). The doping concentrations are evaluated by electro-chemical capacitance voltage measurements (ECV) and the localization verified, together with stoichiometry, by atom probe tomography (APT), see Fig. 1. The composition from a central part with five quantum wells is shown in Fig. 1a. Reconstructed APT elemental maps are provided in Fig. 1b-f. The GeSn wells, forming the active region, have a Sn concentration of 8.6% which was confirmed by Rutherford backscattering spectrometry (RBS), and a thickness of about 19 nm for each of the seven wells. By switching the Si flux on during barrier growth, 10.5% Si is incorporated into the roughly 11 nm thick barrier layers. The Si atoms are well confined within the SiGeSn barrier layers, where a slight Sn content increase can also be observed: adding Si modifies the incorporated Sn concentration, which increases here to 10.9% Sn¹⁹. Based on APT, the location of p-dopants and separation of n-dopants from the first barrier is also verified (Fig. 1e, f). It should be noted that, Phosphorus atoms which can be seen in the measurement above the n-doped layer are noise due to the measurement. In contrast, the GeSn homojunction LED, used for comparison, consists of a 514 nm thick $\text{Ge}_{0.915}\text{Sn}_{0.085}$ layer with a residual compressive strain of -0.2%, determined by X-ray diffraction reciprocal space mapping. The n- and p-doping amounts to $7 \cdot 10^{19} \text{ cm}^{-3}$ and $3 \cdot 10^{18} \text{ cm}^{-3}$, respectively.

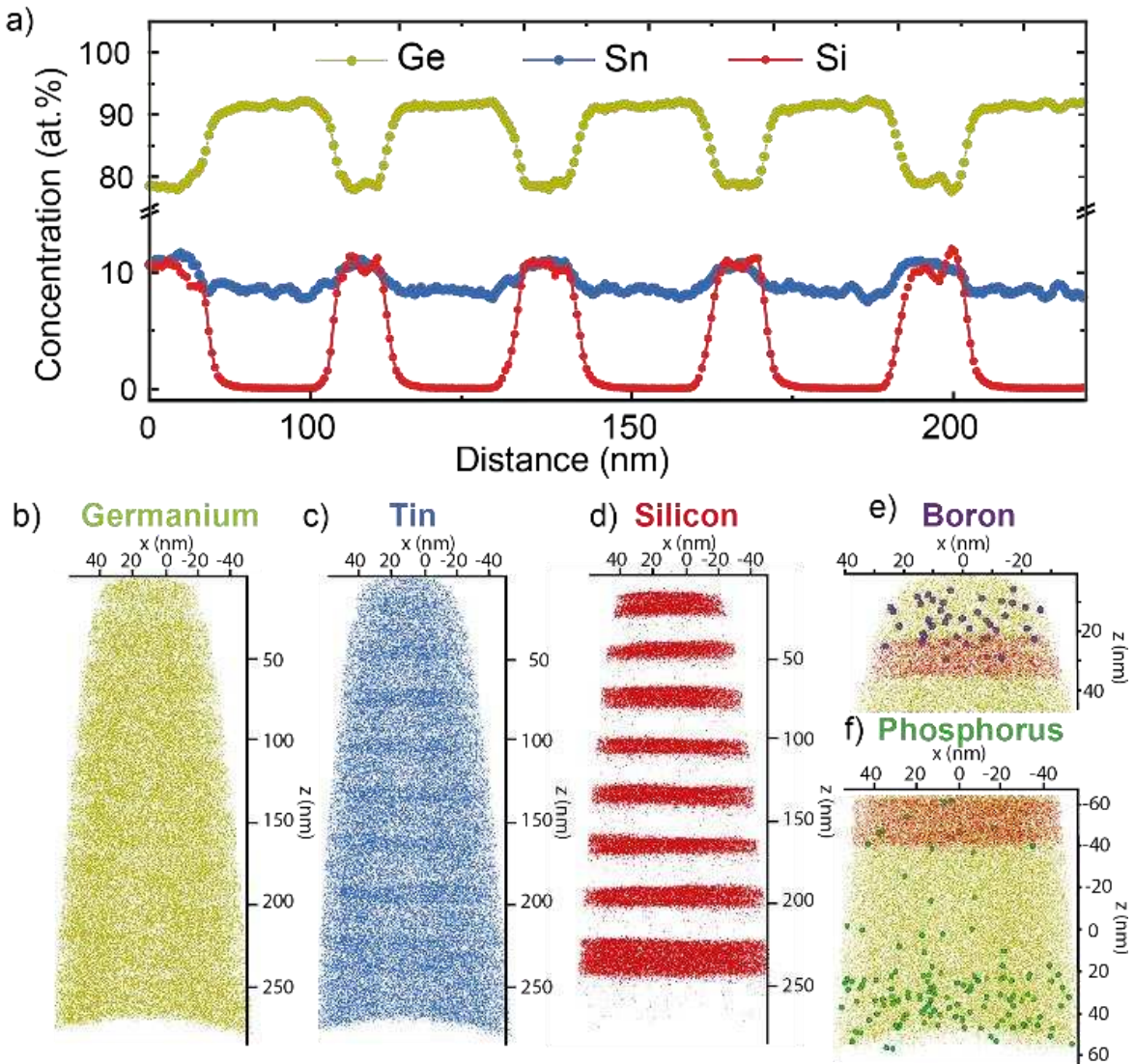


Fig. 1. a) APT concentration profiles across a central part of the MQW LED. APT elemental maps of the GeSn/SiGeSn MQW: individual maps for Ge, Sn and Si are provided in b)-d). The B atoms in the GeSn:B layer on top of the MQW appear as violet dots in the top part of Fig. e). The P atoms in the bottom Ge:P layer which is ~ 60 nm beneath the first SiGeSn barrier appear as dark green dots in the bottom part of Fig. f).

The light emitting devices are fabricated using standard clean room silicon CMOS processing. The structures are defined by optical photolithography. Mesas are patterned and contact windows are opened by reactive ion etching with Cl_2/Ar , and CHF_3 plasmas. Surface passivation is assured by ~ 150 nm SiO_2 deposited using plasma enhanced CVD at 300°C . Low resistance metallic NiGeSn layers²⁰, together with 200 nm sputtered Al, form the metallic contacts. A schematic of a fabricated device is presented in Fig. 2a.

To investigate the MQW structure confinement properties, the bulk alloys band structures²¹ were first calculated (using 8-band k.p model at Γ), with strain effects described via deformation potentials²², and were then used to find the band alignment in MQWs¹⁴, shown in Fig. 2b,c. The compressive strain in the wells makes them more indirect. Calculations for the GeSn well give an energy separation between L- and Γ -valley in the conduction band of just $\Delta E = -4$ meV for the slightly indirect material. Two GeSn/SiGeSn band structures, one with a $b_{\text{SiSn},\Gamma} = 19$ eV²³ bowing parameter at the Γ -point (Fig. 2b) and the other with $b_{\text{SiSn},\Gamma} = 3.9$ eV¹⁴ (Fig. 2c), were then computed (in order to account for the spread in literature values). The same $b_{\text{SiSn},L} = 2.124$ eV¹⁴ value at the L point was used in both cases. The {GeSn/SiGeSn} configuration investigated here was chosen so that it always provides type-I band alignment, irrespectively of the Γ -valley SiSn bowing parameter used. As seen in Fig. 2b,c, both electrons and holes are confined in the GeSn wells, which should lead to large improvement in the radiative recombination rate. This situation is not fulfilled for most GeSn/Ge MQW configurations, as detailed in Ref¹¹. Note that the strong dependence of Γ -valley on the SiSn bowing parameter results more rapidly in direct bandgaps for higher $b_{\text{SiSn},\Gamma}$ values. With $b_{\text{SiSn},\Gamma} = 19$ eV, the bandgap of the SiGeSn ternary alloy used here, is actually direct. However, even in this case the structure maintains its required properties: significantly larger bandgap in the SiGeSn barriers than in the GeSn wells, and type I band alignment. Clearly, the band structure of SiGeSn has to be investigated in more detail in order to match calculations and experimental data. With the large dispersion of the reported values of SiSn bowing parameters, it is likely that more than a simple quadratic interpolation of conventional binary bowing terms is necessary for the ternary. Because of these uncertainties in band structure calculations, only the experiment can reveal the extent of carrier confinement.

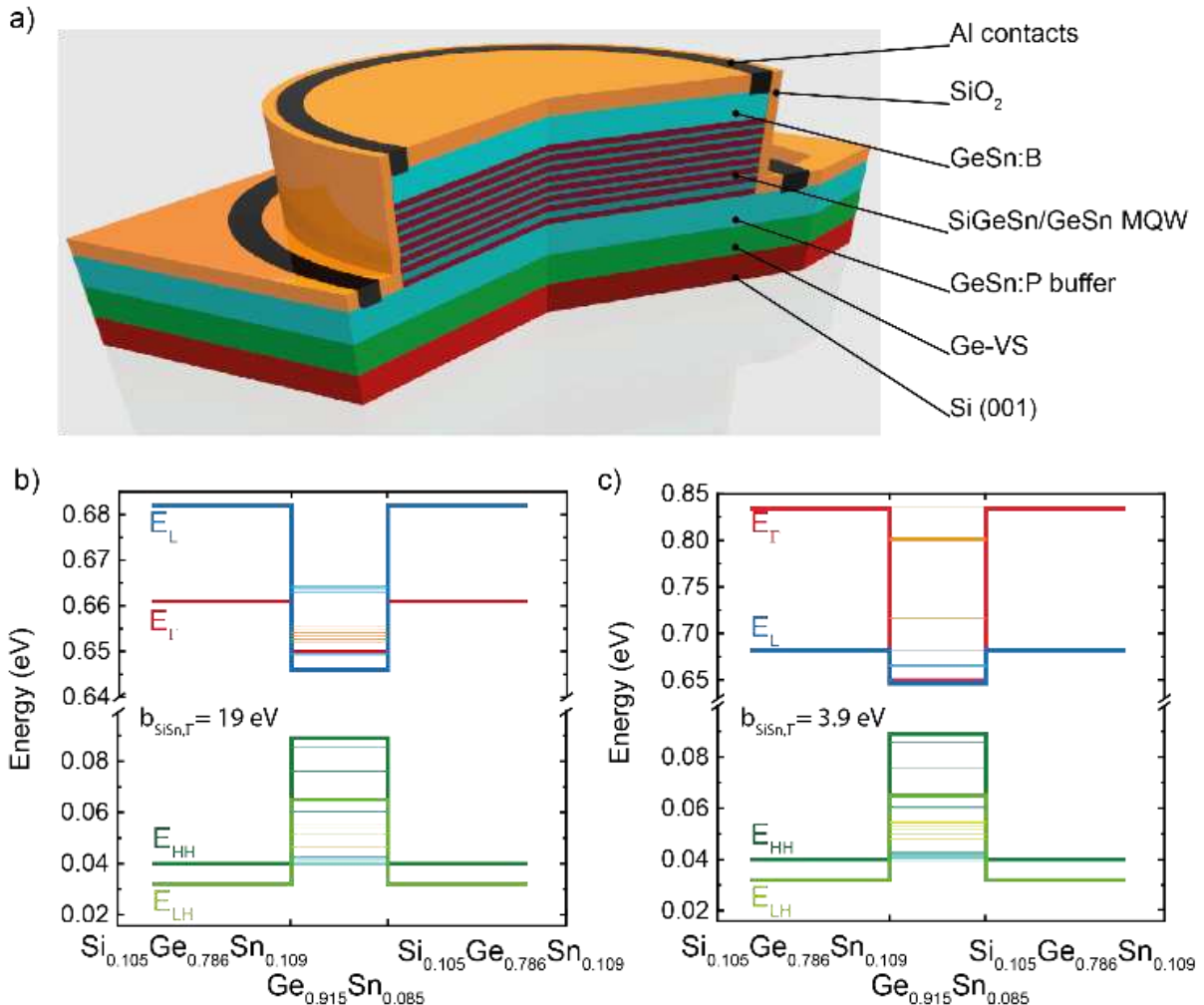


Fig. 2. (a) Schematic of a GeSn/SiGeSn MQW LED. Calculated electronic band structure of the associated GeSn/SiGeSn quantum well structure with either high b) or low c) SiSn bowing parameters.

Electroluminescence is recorded using a Vertex 80v Bruker spectrometer in a step scan mode. The sample is mounted in a He-cooled finger cryostat enabling temperature dependent analysis. A modulated, rectangular voltage is applied with a repetition rate of ~ 2 kHz and a duty cycle (DC) of 50%. The emitted light is detected by a liquid nitrogen cooled InSb detector with an optical filter with a cutoff wavelength of 3 μm mounted in front. Spectra of the GeSn/SiGeSn MQW structure (blue) and of the GeSn homojunction (green, dashed) collected at 4 K (left) and 300 K (right) are shown in Fig. 3a. The peak current density j , matched for both devices, is about 150 A/cm 2 . At both temperatures, the light emission yield of the MQW structure is definitely higher than that of the homojunction. At low temperatures, where non-radiative recombination paths are reduced, the intensity is tremendously enhanced. Temperature dependent measurements of both LED devices show that the electroluminescence intensity increases strongly as the temperature decreases. This rise is obvious in Fig. 3b where the normalized intensities of the GeSn/SiGeSn MQW (full squared symbols) and the GeSn homojunction (empty circle symbols) are compared between 4 K and 300 K. Integrated intensities are normalized to room temperature values. The strong MQW LED emission increase compared to homojunction at low temperatures may be attributed to the type I band alignment which yields an efficient confinement of electrons and holes in the wells. More carriers are then available for band-to-band recombination in the active material than in the homojunction case. Moreover, a GeSn alloy with a smaller energy offset between L and Γ has a higher ratio of electrons at Γ , resulting in a higher radiative band-to-band recombination rate. An effect of quantization on the EL emission cannot be resolved and is not intended since quantization effects would transform the alloy to a more indirect one. EL peak energy positions and full width at half maximum (FWHM) were extracted from the spectra and provided in Fig. 3c. The MQW spectra show (i) a Varshni-like increase of the EL peak energy with decreasing temperature (empty squared symbols) and (ii) a steady broadening of the FWHM (full squared symbols) as the temperature increases. The peak positions of spectra collected from a homojunction LED are plotted as green empty circles in Fig. 3c. Despite the comparable strain values in the active regions, the emission energy of the homojunction lies 20 meV above the emission energy of the MQW device, which is a clear sign that the bandgap is slightly smaller in the latter. Measurement inaccuracies concerning the Sn concentration ($\pm 0.5\%$) and strain ($\pm 0.1\%$) may explain this discrepancy.

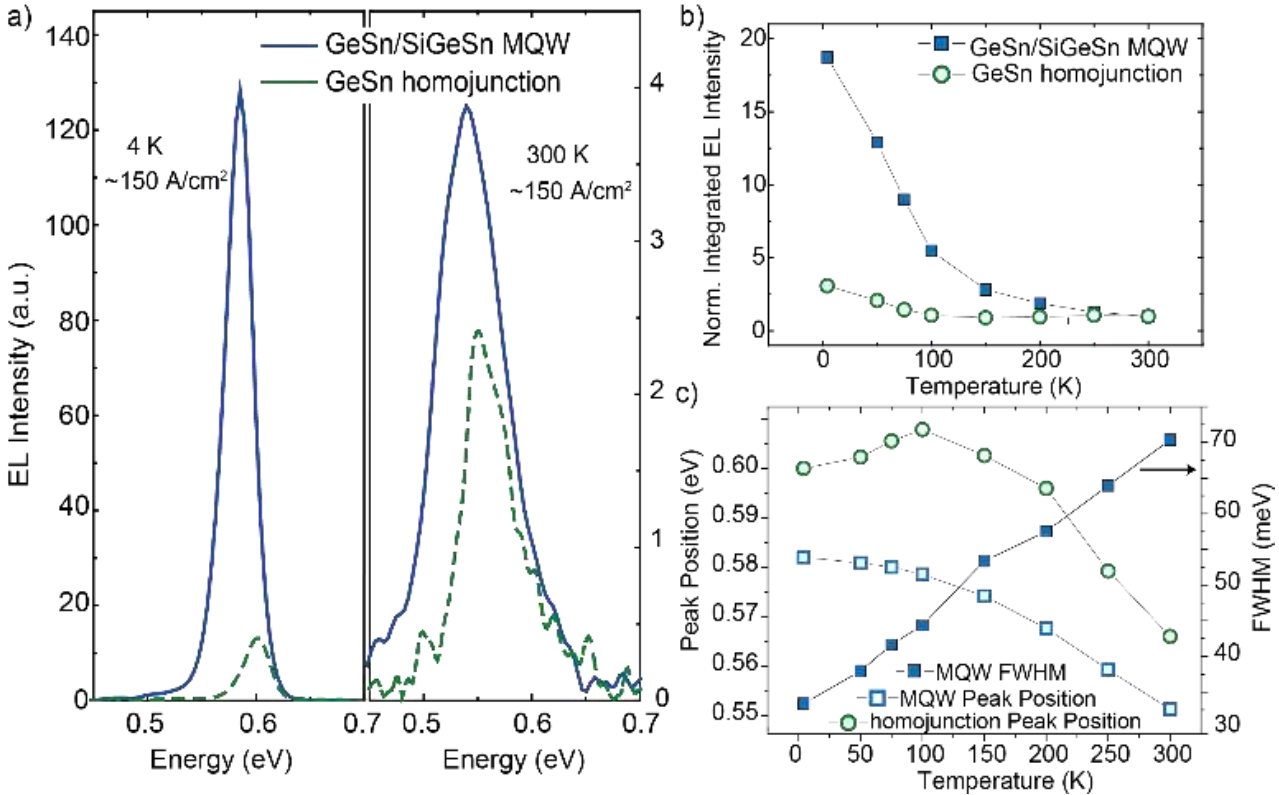


Fig. 3. (a) Emission spectra at 4 K and 300 K of $d = 100 \mu\text{m}$ GeSn/SiGeSn MQW (blue) and homojunction (green, dashed) LEDs. (b) Integrated intensity of both LEDs as a function of temperature for $j = 250 \text{ Acm}^{-2}$ normalized to the values at 300 K. (c) FWHM (for the MQW) and peak position (homojunction and MQW) at different temperatures.

Power dependence of the light emission from the GeSn/SiGeSn MQW device is also investigated. Figure 4a shows EL spectra at temperatures of 4 K and 300 K as inset for various injection current densities. The current density values given in Fig. 4a correspond to the applied peak current densities. As expected, the EL intensities increase with the current densities (from 0.8 up to 223 A/cm 2 at 4 K). The integrated EL intensity is shown as a function of current density for different temperatures in Fig. 4b. In line with temperature dependence shown in Fig. 3b, the EL intensities at low temperature are higher than that at room temperature. At $T = 4$ K the slope of the power dependence on a log-log scale in Fig. 4b is around 0.3 for low injection (e.g. $j < 5 \text{ A/cm}^2$), an injection regime in which the limiting process might be trap assisted non-radiative recombination paths. It increases to 0.6 for larger

injection currents, suggesting Auger recombination²⁴ in the layer. At higher temperatures, the radiative recombination seems to be dominated by direct band-to-band recombination, then the slope of the current dependence of the EL approaches the value of 1.0. The EL peak positions are analyzed and displayed in Fig. 4c as functions of the current density, for four temperatures. The peak position is almost constant over the whole current density range at every temperature probed. At higher temperatures the decrease of peak energy is below 5 meV, indicating the absence of any significant heating in the device. Duty cycle (DC) dependent EL is also investigated at 15 K in a 150 μm diameter MQW LED for $j = 194 \text{ A/cm}^2$. The repetition rate was kept at 2 kHz. To investigate the impact of heating due to large power supplied to the diodes, the peak position was measured as a function of DC, shown in Fig. 4d (empty squares). The peak position remains constant at 583 meV, irrespectively of the DC. The EL intensity has a maximum at 50% DC, and varies linearly in either direction off this point. The maximum is just an effect of the lock-in amplifier measurements of the first term of the Fourier transformation. Both, the constant peak of the EL spectra and the linear dependence of the EL intensity position with DC are clear hints that heating is negligible. These are important findings regarding the devices' temperature stability.

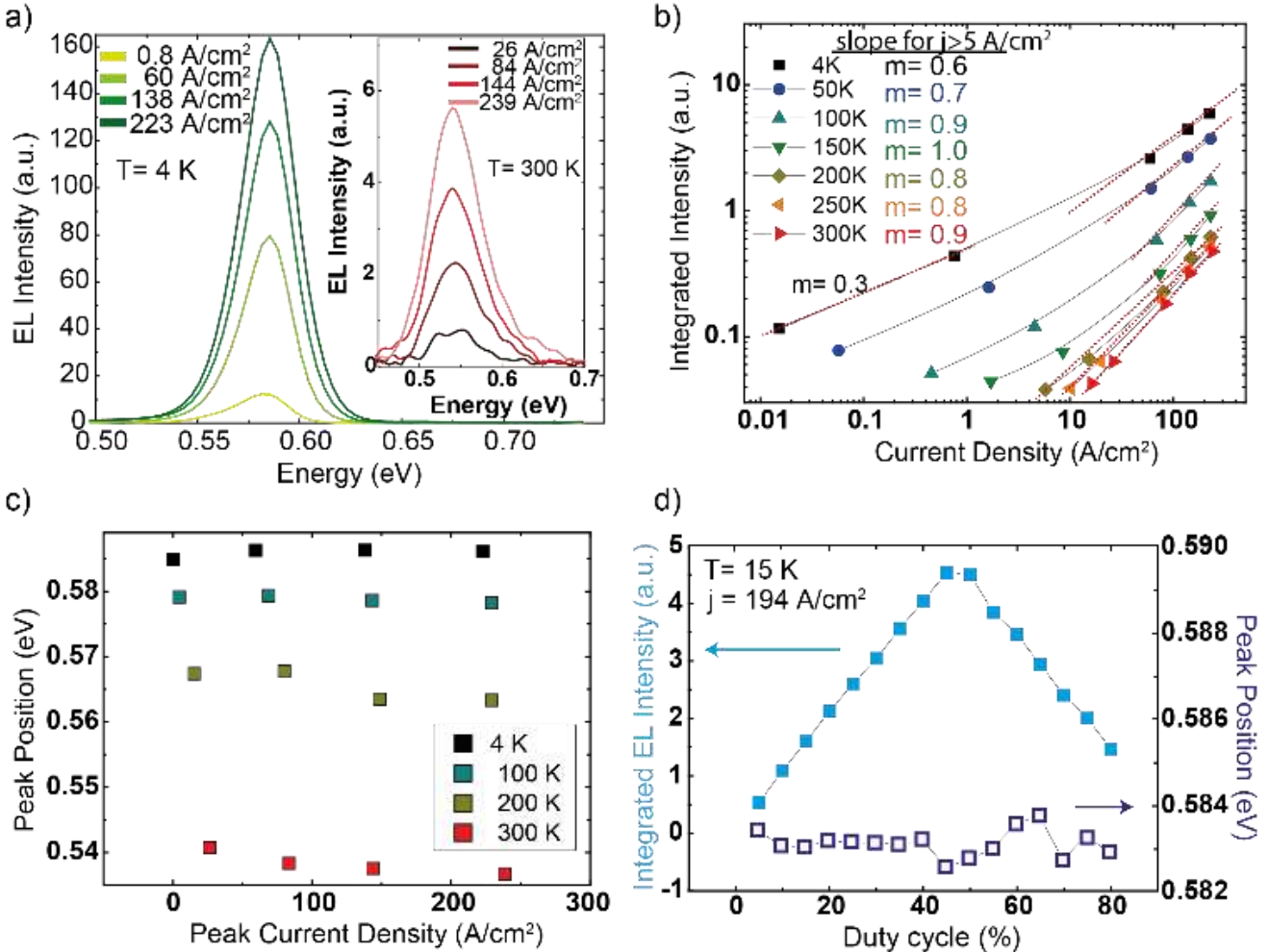


Fig. 4. a) EL spectra for different peak current densities j at 4 K and 300 K (inset). b) the integrated intensity of a GeSn/SiGeSn MQW device plotted as a function of j at different temperatures. c) EL peak position as a function of j at different temperatures. d) Integrated EL intensity and peak position at 15 K as functions of the duty cycle.

In conclusion, we showed strongly improved MQW LED performance compared to homojunction devices. The temperature dependence clearly highlights the influence of SiGeSn barrier material for efficient carrier confinement in heterostructures, however compositions with even stronger confinement would be favorable for operation at room temperature. Further analysis of the MQW LED was provided by power dependent EL measurements below 500 A/cm^2 . Heating, expected to occur with increased injection currents, has no impact on optical properties underlining temperature stability of the presented devices. The on-going improvement of material quality will lead to decreased trap assisted recombination, offering higher efficiency at low injection. In addition, the use of a direct bandgap MQW structure with SiGeSn as barrier material will lead to a higher density of confined Γ -electrons and thus efficient light emission, which is also a prerequisite for electrically pumped GeSn lasers.

Funding. DFG project “SiGeSn Laser for Silicon Photonics”. Villum Foundation. Romanian National Authority for Scientific Research and Innovation, (CCCDI – UEFISCDI, project No. 58 / 2016), in the frame of the EU project M.ERANET-3107-GESNAPHOTO.

Acknowledgment. We thank the Helmholtz Nano Facility (HNF) team for cleanroom support and service.

REFERENCES

1. D. J. Richardson, *Nat. Photonics* **3**, 562 (2009).
2. D. J. Thomson, L. Shen, J. J. Ackert, E. Huante-Ceron, A. P. Knights, M. Nedeljkovic, A. C. Peacock, and G. Z. Mashanovich, *Opt. Express* **22**, 10825 (2014).
3. P. Moontragoon, Z. Ikonić, and P. Harrison, *Semicond. Sci. Technol.* **22**, 742 (2007).
4. S. Wirths, R. Geiger, N. von den Driesch, G. Mussler, T. Stoica, S. Mantl, Z. Ikonic, M. Luysberg, S. Chiussi, J. M. Hartmann, H. Sigg, J. Faist, D. Buca, and D. Grützmacher, *Nat. Photonics* **9**, 88 (2015).
5. D. Stange, S. Wirths, R. Geiger, C. Schulte-Braucks, B. Marzban, N. von den Driesch, G. Mussler, T. Zabel, T. Stoica, J.-M. Hartmann, S. Mantl, Z. Ikonic, D. Grützmacher, H. Sigg, J. Witzens, and D. Buca, *ACS Photonics* **3**, 1279–1285 (2016).
6. C. N. Boswell-koller, P. R. Stone, O. D. Dubon, A. M. Minor, M. Watanabe, J. W. Beeman, K. M. Yu, J. W. A. Iii, D. C. Chrzan, and E. E. Haller, *Nano Lett.* **10**, 2794 (2010).
7. J. D. Gallagher, C. L. Senaratne, P. M. Wallace, J. Menéndez, and J. Kouvetsakis, *Appl. Phys. Lett.* **107**, 123507 (2015).
8. M. Oehme, K. Kostecki, T. Arguirov, G. Mussler, K. Ye, M. Gollhofer, M. Schmid, M. Kaschel, R. A. Körner, M. Kittler, D. Buca, E. Kasper, and J. Schulze, *IEEE Photonics Technol. Lett.* **26**, 2013 (2014).
9. Y. Zhou, W. Dou, W. Du, T. Pham, S. A. Ghemirri, S. Al-Kabi, A. Mosleh, M. Alher, J. Margetis, J. Tolle, G. Sun, R. Soref, B. Li, M. Mortazavi, H. Naseem, and S.-Q. Yu, *J. Appl. Phys.* **120**, 023102 (2016).
10. B. Schwartz, M. Oehme, K. Kostecki, D. Widmann, M. Gollhofer, R. Koerner, S. Bechler, I. A. Fischer, T. Wendav, E. Kasper, J. Schulze, and M. Kittler, *Opt. Lett.* **40**, 3209 (2015).
11. D. Stange, N. von den Driesch, D. Rainko, C. Schulte-Braucks, S. Wirths, G. Mussler, A. T. Tiedemann, T. Stoica, J. M. Hartmann, Z. Ikonic, S. Mantl, D. Grützmacher, and D. Buca, *Opt. Express* **24**, 1358 (2016).
12. Z. Alferov, *IEEE J. Sel. Top. Quantum Electron.* **6**, 832 (2000).
13. C. L. Senaratne, P. M. Wallace, J. D. Gallagher, P. E. Sims, J. Kouvetsakis, and J. Menéndez, *J. Appl. Phys.* **120**, 025701 (2016).
14. P. Moontragoon, R. A. Soref, and Z. Ikonic, *J. Appl. Phys.* **112**, 073106 (2012).
15. G. Sun, R. A. Soref, and H. H. Cheng, *J. Appl. Phys.* **108**, 033107 (2010).
16. G.-E. Chang, S.-W. Chang, and S. L. Chuang, *Opt. Express* **17**, 11246 (2009).
17. T. Wendav, I. A. Fischer, M. Montanari, M. H. Zoellner, W. Klesse, G. Capellini, N. von den Driesch, M. Oehme, D. Buca, K. Busch, and J. Schulze, *Appl. Phys. Lett.* **108**, 242104 (2016).
18. J. M. Hartmann, A. Abbadie, N. Cherkashin, H. Grampeix, and L. Clavelier, *Semicond. Sci. Technol.* **24**, 055002 (2009).
19. S. Wirths, D. Buca, Z. Ikonic, P. Harrison, a. T. Tiedemann, B. Holländer, T. Stoica, G. Mussler, U. Breuer, J. M. Hartmann, D. Grützmacher, and S. Mantl, *Thin Solid Films* **557**, 183 (2014).
20. S. Wirths, R. Troitsch, G. Mussler, J.-M. Hartmann, P. Zaumseil, T. Schroeder, S. Mantl, and D. Buca, *Semicond. Sci. Technol.* **30**, 055003 (2015).
21. T. B. Bahder, *Phys. Rev. B* **41**, 11992–12001 (1990).
22. G.-E. Chang, S.-W. Chang, and S. L. Chuang, *IEEE J. Quantum Electron.* **46**, 1813–1820 (2010).
23. N. von den Driesch, D. Stange, S. Wirths, D. Rainko, I. Povstugar, A. Savenko, U. Breuer, R. Geiger, H. Sigg, Z. Ikonic, J.-M. Hartmann, D. Grützmacher, S. Mantl, and D. Buca, submitted to *Small* (2016).
24. T. Stoica, L. Vescan, A. Muck, B. Hollander, and G. Schope, *Phys. E* **16**, 359 (2003).

REFERENCES without abbreviations

1. D. J. Richardson, "Silicon photonics: Beating the electronics bottleneck," *Nat. Photonics* **3**, 562–564 (2009).
2. D. J. Thomson, L. Shen, J. J. Ackert, E. Huante-Ceron, A. P. Knights, M. Nedeljkovic, A. C. Peacock, and G. Z. Mashanovich, "Optical detection and modulation at $2\mu\text{m}$ - $2.5\mu\text{m}$ in silicon," *Opt. Express* **22**, 10825–30 (2014).
3. P. Moontragoon, Z. Ikonić, and P. Harrison, "Band structure calculations of Si–Ge–Sn alloys: achieving direct band gap materials," *Semicond. Sci. Technol.* **22**, 742–748 (2007).
4. S. Wirths, R. Geiger, N. von den Driesch, G. Mussler, T. Stoica, S. Mantl, Z. Ikonic, M. Luysberg, S. Chiussi, J. M. Hartmann, H. Sigg, J. Faist, D. Buca, and D. Grützmacher, "Lasing in direct-bandgap GeSn alloy grown on Si supplementary," *Nat. Photonics* **9**, 88–92 (2015).
5. D. Stange, S. Wirths, R. Geiger, C. Schulte-Braucks, B. Marzban, N. von den Driesch, G. Mussler, T. Zabel, T. Stoica, J.-M. Hartmann, S. Mantl, Z. Ikonic, D. Grützmacher, H. Sigg, J. Witzens, and D. Buca, "Optically Pumped GeSn Microdisk Lasers on Si," *ACS Photonics* **3**, 1279–1285 (2016).
6. C. N. Boswell-koller, P. R. Stone, O. D. Dubon, A. M. Minor, M. Watanabe, J. W. Beeman, K. M. Yu, J. W. A. Iii, D. C. Chrzan, and E. E. Haller, "Embedded Binary Eutectic Alloy Nanostructures : A New Class of Phase Change Materials," *Nano Lett.* **10**, 2794–2798 (2010).
7. J. D. Gallagher, C. L. Senaratne, P. M. Wallace, J. Menéndez, and J. Kouvetsakis, "Electroluminescence from $\text{Ge}_{1-y}\text{Sn}_y$ diodes with degenerate pn junctions," *Appl. Phys. Lett.* **107**, 123507 (2015).
8. M. Oehme, K. Kostecki, T. Arguirov, G. Mussler, K. Ye, M. Gollhofer, M. Schmid, M. Kaschel, R. A. Körner, M. Kittler, D. Buca, E. Kasper, and J. Schulze, "GeSn Heterojunction LEDs on Si Substrates," *IEEE Photonics Technol. Lett.* **26**, 2013–2015 (2014).
9. Y. Zhou, W. Dou, W. Du, T. Pham, S. A. Ghemirri, S. Al-Kabi, A. Mosleh, M. Alher, J. Margetis, J. Tolle, G. Sun, R. Soref, B. Li, M. Mortazavi, H. Naseem, and S.-Q. Yu, "Systematic study of GeSn heterostructure-based light-emitting diodes towards mid-infrared applications," *J. Appl. Phys.* **120**, 23102 (2016).
10. B. Schwartz, M. Oehme, K. Kostecki, D. Widmann, M. Gollhofer, R. Koerner, S. Bechler, I. A. Fischer, T. Wendav, E. Kasper, J. Schulze, and M. Kittler, "Electroluminescence of GeSn/Ge MQW LEDs on Si substrate," *Opt. Lett.* **40**, 3209 (2015).
11. D. Stange, N. von den Driesch, D. Rainko, C. Schulte-Braucks, S. Wirths, G. Mussler, A. T. Tiedemann, T. Stoica, J. M. Hartmann, Z. Ikonic, S. Mantl, D. Grützmacher, and D. Buca, "Study of GeSn based heterostructures: towards optimized group IV MQW LEDs," *Opt. Express* **24**, 1358

- (2016).
12. Z. Alferov, "Double heterostructure lasers: early days and future perspectives," *IEEE J. Sel. Top. Quantum Electron.* **6**, 832–840 (2000).
 13. C. L. Senaratne, P. M. Wallace, J. D. Gallagher, P. E. Sims, J. Kouvettakis, and J. Menéndez, "Direct gap Ge_{1-y}Sn_y alloys: Fabrication and design of mid-IR photodiodes," *J. Appl. Phys.* **120**, 25701 (2016).
 14. P. Moontragoon, R. A. Soref, and Z. Ikonik, "The direct and indirect bandgaps of unstrained Si_xGe_{1-x-y}Sn_y and their photonic device applications," *J. Appl. Phys.* **112**, 73106 (2012).
 15. G. Sun, R. A. Soref, and H. H. Cheng, "Design of an electrically pumped SiGeSn/GeSn/SiGeSn double-heterostructure midinfrared laser," *J. Appl. Phys.* **108**, 33107 (2010).
 16. G.-E. Chang, S.-W. Chang, and S. L. Chuang, "Theory for n-type doped, tensile-strained Ge-Si_xGe_ySn_{1-x-y} quantum-well lasers at telecom wavelength," *Opt. Express* **17**, 11246 (2009).
 17. T. Wendav, I. A. Fischer, M. Montanari, M. H. Zoellner, W. Klesse, G. Capellini, N. von den Driesch, M. Oehme, D. Buca, K. Busch, and J. Schulze, "Compositional dependence of the band-gap of Ge_{1-x-y}Si_xSn_y alloys," *Appl. Phys. Lett.* **108**, 242104 (2016).
 18. J. M. Hartmann, A. Abbadie, N. Cherkashin, H. Grampeix, and L. Clavelier, "Epitaxial growth of Ge thick layers on nominal and 6° off Si(001); Ge surface passivation by Si," *Semicond. Sci. Technol.* **24**, 55002 (2009).
 19. S. Wirths, D. Buca, Z. Ikonik, P. Harrison, a. T. Tiedemann, B. Holländer, T. Stoica, G. Mussler, U. Breuer, J. M. Hartmann, D. Grützmacher, and S. Mantl, "SiGeSn growth studies using reduced pressure chemical vapor deposition towards optoelectronic applications," *Thin Solid Films* **557**, 183–187 (2014).
 20. S. Wirths, R. Troitsch, G. Mussler, J.-M. Hartmann, P. Zaumseil, T. Schroeder, S. Mantl, and D. Buca, "Ternary and quaternary Ni(Si)Ge(Sn) contact formation for highly strained Ge p- and n-MOSFETs," *Semicond. Sci. Technol.* **30**, 55003 (2015).
 21. T. B. Bahder, "Eight-band k · p model of strained zinc-blende crystals," *Phys. Rev. B* **41**, 11992–12001 (1990).
 22. G.-E. Chang, S.-W. Chang, and S. L. Chuang, "Strain-Balanced Ge_zSn_{1-z}-SixGeySn_{1-x-y} Multiple-Quantum-Well Lasers," *IEEE J. Quantum Electron.* **46**, 1813–1820 (2010).
 23. N. von den Driesch, D. Stange, S. Wirths, D. Rainko, I. Povstugar, A. Savenko, U. Breuer, R. Geiger, H. Sigg, Z. Ikonik, J.-M. Hartmann, D. Grützmacher, S. Mantl, and D. Buca, "SiGeSn ternaries for efficient group IV heterostructure light emitters", submitted to Small (2016).
 24. T. Stoica, L. Vescan, A. Muck, B. Hollander, and G. Schope, "Electroluminescence study on electron hole plasma in strained SiGe epitaxial layers," *Phys. E* **16**, 359–365 (2003).